Metal-insulator-metal diodes based on alkyltrichlorosilane self-assembled monolayers

Jidong Jin (iD), Lei Wang, Zhaoliang Zheng, Jiawei Zhang, Xuzhi Hu (iD), Jian R. Lu, David Etor, Chris Pearson, Aimin Song (iD), David Wood, Andrew J. Gallant, and Claudio Balocco

View Online   Export Citation   CrossMark

ARTICLES YOU MAY BE INTERESTED IN

AIP Advances

AVS Quantum Science
Co-published with AIP Publishing
Coming Soon!

Metal-insulator-metal diodes based on alkyltrichlorosilane self-assembled monolayers

View Online   Export Citation   CrossMark

Jidong Jin,[1] [iD] Lei Wang,[1] Zhaoliang Zheng,[2] Jiawei Zhang,[3] Xuzhi Hu,[4] [iD] Jian R. Lu,[4] David Etor,[5] Chris Pearson,[1] Aimin Song,[3] [iD] David Wood,[6] Andrew J. Gallant,[1] and Claudio Balocco[1,a)]

AFFILIATIONS

[1]Department of Engineering, Durham University, Durham DH1 3LE, United Kingdom
[2]Stephenson Institute of Renewable Energy and Department of Chemistry, University of Liverpool, Liverpool L69 7ZD, United Kingdom
[3]School of Electrical and Electronic Engineering, University of Manchester, Manchester M13 9PL, United Kingdom
[4]Biological Physics Group, School of Physics and Astronomy, University of Manchester, Manchester M13 9PL, United Kingdom
[5]Department of Electrical and Computer Engineering, Baze University, Abuja 900108, Nigeria
[6]Faculty of Engineering and Environment, Northumbria University, Newcastle upon Tyne NE1 8ST, United Kingdom

[a)]Author to whom correspondence should be addressed. Electronic mail: claudio.balocco@durham.ac.uk

ABSTRACT

This paper reports on the experimental investigation of metal-insulator-metal (MIM) diodes based on alkyltrichlorosilane self-assembled monolayers (SAMs) with different alkyl chain lengths. The insulating SAM is sandwiched between two metal contacts, Pt and Ti, with different work functions. The electronic properties of the MIM diodes can be tuned by controlling the alkyl chain length of the SAMs to address different constraints in high speed electronics applications. Data fitting of the tunneling current through the MIM junctions using the Fowler-Nordheim model suggests that the device operation is influenced by the barrier heights of the diodes and thicknesses of the SAMs. The current-voltage characteristics achieved in MIM diodes based on alkyltrichlorosilane SAMs make them promising candidates for high speed electronics applications.

Since the first theoretical prediction of molecular rectifiers in 1974,[1] significant attention has been directed to developing diodes based on either single molecules[2–6] or self-assembled monolayers (SAMs).[7–12] Unlike the use of single molecules, the use of SAMs as a dielectric layer appears particularly promising for metal-insulator-metal (MIM) diodes due to their low cost, ease of processing, and compatibility with large-scale manufacturing.[11–14] The operation of an MIM diode is based on quantum mechanical tunneling through a thin dielectric layer between two metal contacts.[15–17] The tunneling of electrons occurring in the MIM diode is a fast process, typically in the femtosecond range,[16,18] and theoretically can rectify frequencies as high as several hundreds of THz.[18] Hence, MIM diodes can operate at much faster speed than conventional Schottky diodes[11] and have been extensively investigated for various high speed electronics applications including energy harvesting[11,19–21]

and infrared detection.[22–24] The design of high-performance MIM diodes requires an ultra-thin high quality dielectric layer to engineer the tunneling current,[15,25] and a large difference in work functions of the metals in order to achieve a sufficient level of nonlinearity and asymmetry.[16,26,27]

Alkyltrichlorosilane ($SiCl_3$-$(CH_2)_{n-1}$-CH_3) SAMs are ultra-thin high quality dielectric films with well-controlled structure.[28–32] MIM diodes based on alkyltrichlorosilane SAMs were initially investigated using metal contacts with similar work functions.[33,34] Recently, MIM diodes based on one of the alkyltrichlorosilane SAMs, octadecyltrichlorosilane with different work function metal contacts have been reported to achieve good rectification characteristics.[13,14] Nevertheless, the diodes based on octadecyltrichlorosilane may not provide optimal performance for high-speed electronics applications, since the layer thickness and surface roughness of the SAM are
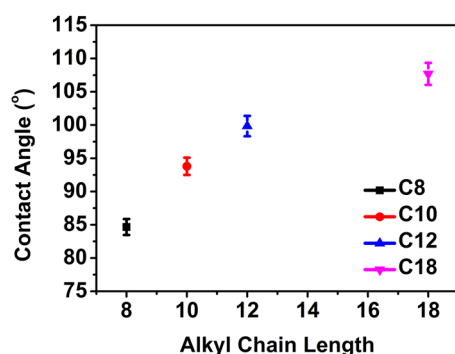
FIG. 1. Water contact angle as a function of alkyl chain length. Six different locations were measured and the error bars represent the standard deviations from measurements between repeated samples.

highly dependent on many factors, in particular, the alkyl chain length,[35,36] which will influence the diode performance. Hence, further refinement is possible in order to optimize the SAMs used for the diode fabrication. Currently, no systematic study on the realization of MIM diodes using alkyltrichlorosilane SAMs and metal contacts with a large difference in work function exists in the literature.

In this work, we report the use of alkyltrichlorosilane SAMs sandwiched between metal contacts with two dissimilar work functions, Pt (5.65 eV)[16,37] and Ti (4.33 eV),[37] to investigate how the alkyl chain length affects the electrical properties of the MIM diodes. Four SAMs with different chain lengths were used (see supplementary material for structures of alkyltrichlorosilane SAMs), octyltrichlorosilane ($SiCl_3$-$(CH_2)_7$-CH_3, denoted as C8), decyltrichlorosilane ($SiCl_3$-$(CH_2)_9$-CH_3, denoted as C10), dodecyltrichlorosilane ($SiCl_3$-$(CH_2)_{11}$-CH_3, denoted as C12) and octadecyltrichlorosilane ($SiCl_3$-$(CH_2)_{17}$-CH_3, denoted as C18).

To begin with, alkyltrichlorosilane SAMs were formed by submerging the substrates in silane solutions (1 part of alkyltrichlorosilane dissolved in 2000 parts of hexane by volume) for 1 h at room temperature (approximately 21 °C), after which the substrates were rinsed with hexane to remove unbound silanes, and then dried using compressed nitrogen gas. Finally, the substrates were baked for 10 min at 90 °C to complete the surface binding via polymerization and remove any residual solvent. The physical characterization of static contact angle, spectroscopic ellipsometry, and atomic force microscopy (AFM) was carried out for the alkyltrichlorosilane SAMs. Static contact angles were measured with a DSA100 Expert Drop Shape Analyzer (KRÜSS GmbH) to characterize the surface of the alkyltrichlorosilane SAMs on Ti. Droplets of distilled water, with a volume of 5 μL, were placed onto the surface of the SAMs. The contact angles were measured six times at different locations on each film. Spectroscopic ellipsometry (J.A. Woollam Co. Inc) was conducted over the wavelength range 200-1000 nm at three angles of incidence 65°, 70° and 75° to determine the thicknesses of alkyltrichlorosilane SAMs silanized on Si wafers with a 90 nm thermally grown SiO_2 layer. The experimental data was fitted with fixed optical constants (the refractive indices equivalent to the liquid phase of alkane), giving the relative thickness of the layer measured.[37] Measurements were repeated at multiple positions on different films of the same coating. Tapping mode AFM was used to characterize the surface morphology of the alkyltrichlorosilane SAMs silanized on the Si wafer with a 300 nm thermally grown SiO_2 layer. The substrate had a root mean square (rms) roughness of 0.10 nm and the scanned area of the alkyltrichlorosilane SAMs and metal contacts was $1 \times 1 \, \mu m^2$.

The measured water contact angle values for alkyltrichlorosilane molecules with different alkyl chain lengths are shown in Fig. 1. The mean contact angles of C8, C10, C12, and C18 surfaces were found to be 86, 93, 97, and 106°, confirming the hydrophobic nature of the CH_3 terminated surfaces.[34] Higher water contact angles were observed for longer alkyl chain length molecules,
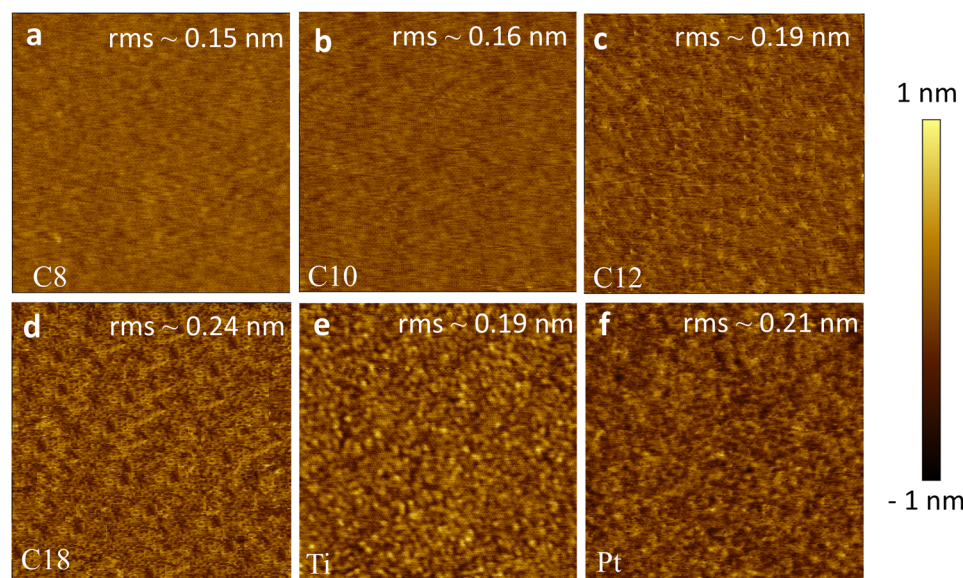
FIG. 2. Tapping mode AFM images (1 μm × 1 μm) from the top surfaces of (a) octyltrichlorosilane (C8), (b) decyltrichlorosilane (C10), (c) dodecyltrichlorosilane (C12), (d) octadecyltrichlorosilane (C18), (e) Ti and (f) Pt.

TABLE I. Main Properties of alkyltrichlorosilane SAMs.

| Alkyltrichlorosilane	Film thickness (nm)	rms roughness (nm)	Mean contact angle (°)
C8	1.20	0.15	86
C10	1.34	0.16	93
C12	1.57	0.19	97
C18	2.23	0.24	106

suggesting higher carbon concentration with lower surface energy.[38] Prior to the SAM deposition, the contact angle of the Ti surface was found to be around 10°, confirming the hydrophilic nature of the OH terminated surface.[13]

Insulator and metal imperfections at the metal/insulator interfaces give rise to conduction other than tunneling.[15] Hence, the production of high quality insulator and metal with smooth interfaces is crucial for high performance MIM diodes. Ellipsometry measurements showed that the thicknesses of C8, C10, C12, and C18 monolayers were 1.20, 1.34, 1.57, and 2.23 nm respectively and that the variation of the thicknesses did not exceed ±0.2 nm for all samples. The rms surface roughnesses of C8, C10, C12, and C18 monolayers were found to be 0.15, 0.16, 0.19, and 0.24 nm, respectively (Fig. 2a–d). The longer alkyl chain molecules had a higher rms surface roughness, consistent with the findings previously reported.[36] These ultra-thin and smooth alkyltrichlorosilane SAMs are expected to lead to low parasitic parallel conduction compared to the conventional oxide dielectric films used in MIM diodes. The rms surface roughnesses of Ti and Pt were 0.19 and 0.21 nm, respectively

(Fig. 2e and 2f), which demonstrates low rms surface roughness of the metal contacts. The thicknesses, rms surface roughnesses, and water contact angles of each of the alkyltrichlorosilane SAM films are summarized in Table I.

The diodes were fabricated on 2-inch Si wafers with a 300 nm thermally grown SiO_2 layer. Standard photolithography was used to pattern the metal contacts. A Moorfield minilab 060 e-beam evaporation system was used for the metal deposition. Figure 3(a) shows the top view and cross-section schematic of the MIM diode (see supplementary material for detailed fabrication process). The alkyltrichlorosilane SAM is sandwiched between two metal contacts, Pt and Ti. The overlapping region between the Ti and Pt contacts determines the effective area of the diode, which is 100 μm^2. The electrical current-voltage (I-V) measurements were conducted with an Agilent E5270B semiconductor parameter analyzer.

The I-V characteristics of MIM diodes with different alkyltrichlorosilane SAMs are shown in Fig. 3b (semi-logarithmic scale I-V) and Fig. 4b–e (linear scale I-V). It can be seen that by decreasing the alkyl chain length, both the reverse and forward currents increase, suggesting that the tunneling probability increases with a decreasing film thickness. From the I-V characteristics, four figures of merit (FOM) such as asymmetry (f_{asym}), dynamic resistance (R_d), nonlinearity (f_{nl}), and responsivity (f_{res}) were extracted in order to evaluate the performance of the diodes. f_{asym} is defined as the ratio of forward to reverse current. $R_d = dV/dI$ and a low value of R_d is generally required for lower power dissipation in the diode. f_{nl} is defined as the ratio of static resistance (V/I) to dynamic resistance R_d, i.e., $f_{nl} = \frac{V}{I}/R_d$. f_{res} is defined as the ratio of the second derivative to the first derivative of the I-V characteristics, i.e., $f_{res} = \frac{d^2I}{dv^2}/\frac{dI}{dV}$.
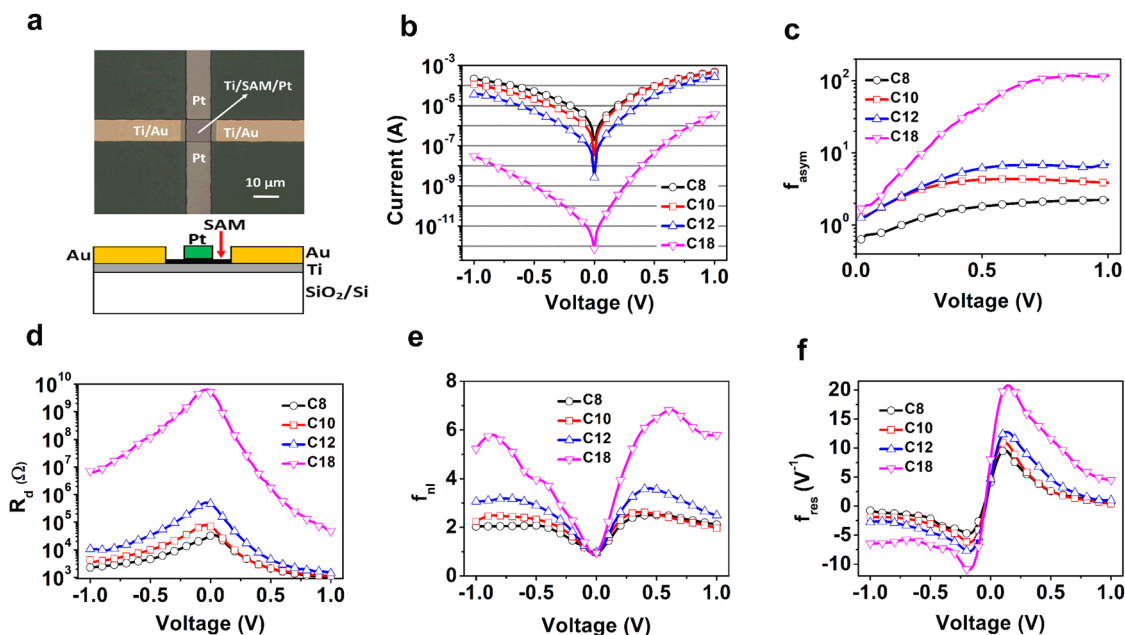
FIG. 3. (a) Top view optical microscope image and cross-section schematic of an MIM diode. (b) Current versus voltage characteristics of MIM diodes based on four different alkyltrichlorosilane SAMs. Extracted (c) asymmetry (f_{asym}), (d) dynamic resistance (R_d), (e) nonlinearity (f_{nl}) and (f) responsivity (f_{res}) of the MIM diodes.
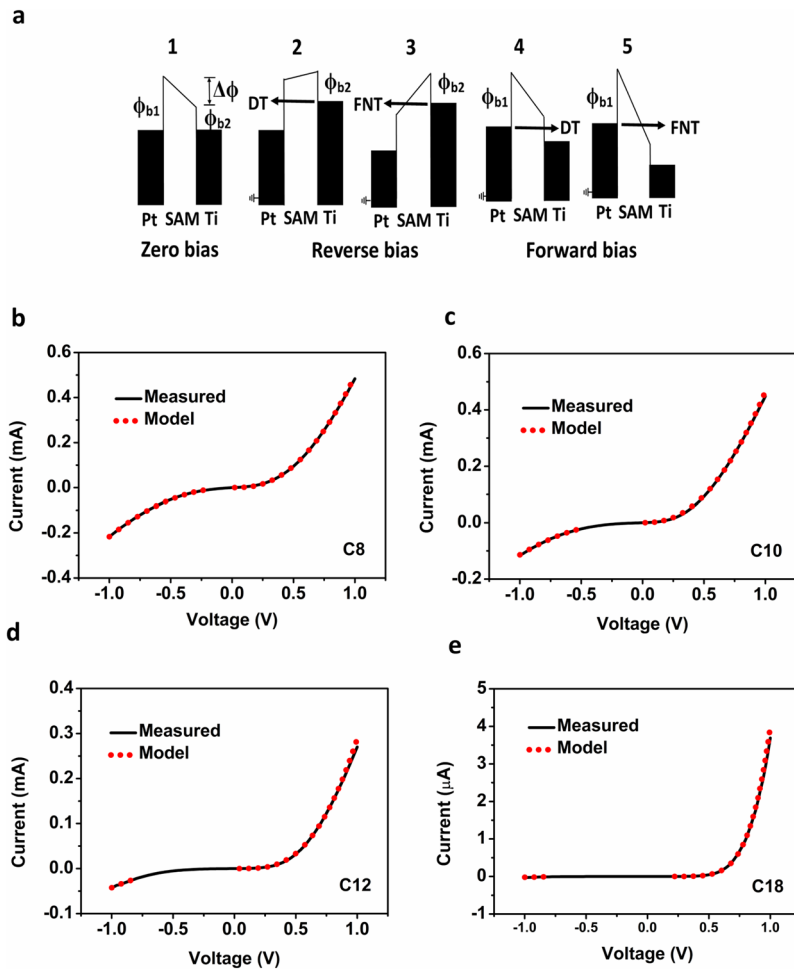
FIG. 4. (a) Energy-band diagrams of the MIM diodes with Ti/SAM/Pt structure. DT and FNT refer to direct and Fowler-Nordheim tunneling and the direction of electron injection is indicated by arrows. Measured and fitted *I-V* curves for the MIM diodes based on four different alkyltrichlorosilane SAMs; (b) octyltrichlorosilane (C8), (c) decyltrichlorosilane (C10), (d) dodecyltrichlorosilane (C12), (e) octadecyltrichlorosilane (C18).

f_{res} is a measure of the diode's rectification ability and is directly related to f_{nl} in the diode's *I-V* characteristic. The higher the f_{nl}, the higher the f_{res}.[24] Ideally, MIM diodes should exhibit *I-V* characteristics with high f_{asym}, f_{nl} and f_{res} for most high speed electronics applications. The extracted electrical properties of the MIM diodes, f_{asym}, R_d, f_{nl}, and f_{res} are shown in Fig. 3c–f. As the thickness of the alkyltrichlorosilane SAMs is varied, a trade-off is apparent between R_d and the other FOM (f_{asym}, f_{nl}, and f_{res}). Consequently, the choice of an optimum MIM device should take into consideration this trade off, depending on the application.

For energy harvesting applications, it is important for the diodes to operate at zero-bias, and for R_d to be low enough in order to minimize the potential mismatch between the impedance of the diodes and the antennas utilized. Hence, the f_{res} and R_d at zero bias were also determined. The zero-bias f_{res} for the diode based on C8, C10, C12, and C18 films were found to be 4.1, 4.6, 4.7, and 8.0 V^{-1}, respectively. In addition, the zero-bias dynamic resistance for the diodes based on C8, C10, C12, and C18 films were found to be 32 kΩ, 71 kΩ, 464 kΩ, and 5 GΩ, respectively. The zero-bias R_d of the diode based on the C18 film was significantly higher than that for a device previously reported by Etor *et al.*[14] This is due to the

improvement in the SAM deposition, resulting in the reduction of the number of defects and ultimately less parasitic parallel conduction. The 15 min sonication step after the formation of the alkyltrichlorosilane SAMs on Ti was removed and the samples were rinsed with hexane, followed by drying using compressed nitrogen gas. It is likely that sonication caused structural changes in the films, leading to a low breakdown voltage of ±0.35 V. All of the diodes could operate in a voltage range of ±1 V without sonication, similar to the diodes based on alkyltrichlorosilane SAMs reported previously.[29,34] Although the diode based on C8 has the lowest zero-bias f_{res} as shown in Fig. 3f, the obtained zero-bias f_{res} value was similar or considerably higher than most MIM diodes typically designed for high speed electronics applications.[24,39] In addition, the diode based on the C8 film has the lowest zero-bias R_d as shown in Fig. 3d, hence this is promising for integration with an antenna for energy harvesting. For applications such as detection and sensing of infrared signals, the MIM diodes can be biased by an external source where high f_{asym}, strong f_{nl} and high f_{res} are the most important considerations rather than zero-bias operation. Figure 3 shows that the diode based on C18 has the highest f_{asym}, strongest f_{nl} and highest f_{res}. The maximum f_{asym}, f_{nl}, and f_{res}

values of the MIM diode based on C18 are 117.8, 6.8 and 20.8 V^{-1} respectively.

The tunneling current between two similar work function electrodes separated by alkyltrichlorosilane SAMs has been evaluated using Simmons theory.[34] Here, the tunneling occurs between two dissimilar work function metal electrodes Pt and Ti, separated by alkyltrichlorosilane SAMs. Schematic energy-band diagrams for these diodes are shown in Fig. 4a. Due to the difference in work functions between Pt and Ti, the conduction electrons in an MIM diode encounter non-identical barriers (ϕ_{b1} and ϕ_{b2}). Hence, there is a difference in barrier height ($\Delta\phi=\phi_{b1}-\phi_{b2}$) at zero bias (sub-panel 1 of Fig. 4a). To bias the device, a voltage was applied to the Ti electrode while the Pt electrode was connected to ground. At low reverse and forward voltages, the direct tunneling (DT) mechanism would dominate where the applied bias is less than the barrier height, as illustrated in subpanels 2 and 4 of Fig. 4a. In contrast, when the applied bias exceeds the barrier height, Fowler-Nordheim tunneling (FNT) becomes dominant, as illustrated in subpanels 3 and 5 of Fig. 4a. This type of field-assisted FNT can be expressed using

$$I = \frac{A(V + \Delta\phi)^2}{d\phi_b} exp\left(\frac{-Bd(\phi_b)^{\frac{3}{2}}}{V + \Delta\phi}\right), \qquad (1)$$

where A and B are constants, V is the applied voltage, d is the barrier thickness and ϕ_b is the barrier height. For a forward bias, $\phi_b=\phi_{b1}$; for a reverse bias, $\phi_b=\phi_{b2}$. To determine the theoretical I-V fit, it is necessary to determine the barrier heights ϕ_{b1} and ϕ_{b2}. We estimated the barrier heights using Fowler-Nordheim plots[40] of $log\left(\left|\frac{I}{(V+\Delta\phi)^2}\right|\right)$ versus $\frac{1}{V+\Delta\phi}$ for both voltage polarities at an optimum value of $\Delta\phi$ (see supplementary material for the barrier height determination). Table II shows the estimated barrier heights of the MIM diodes based on four different alkyltrichlorosilane SAMs.

The fitting of I-V characteristics was performed using the FNT equation (1). The measured I-V characteristics (solid lines) and fits for the FNT region (dots) are shown in Fig. 4b–e. Due to the very low ϕ_{b2}, as shown in Table II, FNT dominates at positive bias for all diodes. For the diodes based on the short alkyl chain length SAM (e.g. C8), DT dominates at very low negative bias due to the very thin dielectric layer.[15] Whereas, when the alkyltrichlorosilane SAM thickness increases, the negative transition voltage from DT to FNT becomes higher due to the increased ϕ_{b1} and the SAM layer becomes thick enough to stand off significant DT current up to the onset of FNT.[15] Clearly, the electron tunneling and device operation are influenced by the barrier heights of the diodes and the thicknesses of the alkyltrichlorosilane SAMs.

TABLE II. Main parameters of MIM diodes estimated from the Fowler-Nordheim tunneling model.

Alkyltrichlorosilane	$\Delta\phi$ (eV)	ϕ_{b1} (eV)	ϕ_{b2} (eV)
C8	0.084	0.263	0.179
C10	0.100	0.287	0.187
C12	0.157	0.422	0.265
C18	0.373	0.448	0.075

In conclusion, we have fabricated MIM diodes comprised of different alkyl chain length alkyltrichlorosilane SAMs sandwiched between two metal contacts, Pt and Ti, with different work functions. The influence of the alkyl chain length on the electrical properties of the MIM diodes was investigated. The results show that as the alkyl chain length of the SAMs varies, a trade-off is apparent between the dynamic resistance and the other three FOM values, asymmetry, nonlinearity and responsivity. The barrier heights of the MIM diodes were estimated from Fowler-Nordheim plots by plotting $log\left(\left|\frac{I}{(V+\Delta\phi)^2}\right|\right)$ versus $\frac{1}{V+\Delta\phi}$ for both voltage polarities at an optimum value of $\Delta\phi$. We found that the electron tunneling and device operation were influenced by the barrier heights of the diodes and the thicknesses of the alkyltrichlorosilane SAMs. This work provides an important guide for the selection of the appropriate alkyltrichlorosilane SAMs in the development of high speed electronics applications.

See supplementary material for structures of alkyltrichlorosilane SAMs, detailed device fabrication process, and method of barrier height determination.

REFERENCES

[1] A. Aviram and M. A. Ratner, Chem. Phys. Lett. **29**(2), 277–283 (1974).

[2] M. Elbing, R. Ochs, M. Koentopp, M. Fischer, C. von Hänisch, F. Weigend, F. Evers, H. B. Weber, and M. Mayor, Proc. Natl. Acad. Sci. U. S. A. **102**(25), 8815 (2005).

[3] I. Díez-Pérez, J. Hihath, Y. Lee, L. Yu, L. Adamska, M. A. Kozhushner, I. I. Oleynik, and N. Tao, Nat. Chem. **1**, 635–641 (2009).

[4] E. Lörtscher, B. Gotsmann, Y. Lee, L. Yu, C. Rettner, and H. Riel, ACS Nano **6**(6), 4931–4939 (2012).

[5] A. Batra, P. Darancet, Q. Chen, J. S. Meisner, J. R. Widawsky, J. B. Neaton, C. Nuckolls, and L. Venkataraman, Nano Lett. **13**(12), 6233–6237 (2013).

[6] S. Siya, R.-B. Gabino, P.-C. Elena, C. Eugenio, C. Juan Carlos, and A. Nicolás, Nanotechnology **26**(29), 291001 (2015).

[7] A. Dhirani, P.-H. Lin, P. Guyot-Sionnest, R. W. Zehner, and L. R. Sita, J. Chem. Phys. **106**(12), 5249–5253 (1997).

[8] C. A. Nijhuis, W. F. Reus, J. R. Barber, M. D. Dickey, and G. M. Whitesides, Nano Lett. **10**(9), 3611–3619 (2010).

[9] C. A. Nijhuis, W. F. Reus, A. C. Siegel, and G. M. Whitesides, J. Am. Chem. Soc. **133**(39), 15397–15411 (2011).

[10] N. Nerngchamnong, L. Yuan, D.-C. Qi, J. Li, D. Thompson, and C. A. Nijhuis, Nat. Nanotechnol. **8**, 113–118 (2013).

[11] M. Celestin, S. Krishnan, S. Bhansali, E. Stefanakos, and D. Y. Goswami, Nano Res. **7**(5), 589–625 (2014).

[12] H. B. Akkerman, P. W. M. Blom, D. M. de Leeuw, and B. de Boer, Nature **441**, 69 (2006).

[13] D. Etor, L. E. Dodd, D. Wood, and C. Balocco, IEEE Trans. Electron Devices **63**(7), 2887–2891 (2016).

[14] D. Etor, L. E. Dodd, D. Wood, and C. Balocco, Appl. Phys. Lett. **109**(19), 193110 (2016).

[15] E. W. Cowell, N. Alimardani, C. C. Knutson, J. F. Conley, D. A. Keszler, B. J. Gibbons, and J. F. Wager, Adv. Mater. **23**(1), 74–78 (2011).

[16] P. Periasamy, H. L. Guthrey, A. I. Abdulagatov, P. F. Ndione, J. J. Berry, D. S. Ginley, S. M. George, P. A. Parilla, and R. P. O'Hayre, Adv. Mater. **25**(9), 1301–1308 (2013).

[17] Q. Cui, M. Sakhdari, B. Chamlagain, H.-J. Chuang, Y. Liu, M. M.-C. Cheng, Z. Zhou, and P.-Y. Chen, ACS Appl. Mater. Interfaces **8**(50), 34552–34558 (2016).

[18] I. Z. Mitrovic, A. D. Weerakkody, N. Sedghi, J. F. Ralph, S. Hall, V. R. Dhanak, Z. Luo, and S. Beeby, Appl. Phys. Lett. **112**(1), 012902 (2018).

[19] S. Grover and G. Moddel, IEEE J. Photovolt. **1**(1), 78–83 (2011).

[20] E. Briones, J. Alda, and F. J. González, Opt. Express **21**(S3), A412–A418 (2013).

[21] G. Jayaswal, A. Belkadi, A. Meredov, B. Pelz, G. Moddel, and A. Shamim, Mater. Today Energy **7**, 1–9 (2018).

[22] P. C. D. Hobbs, R. B. Laibowitz, F. R. Libsch, N. C. LaBianca, and P. P. Chiniwalla, Opt. Express **15**(25), 16376–16389 (2007).

[23] S. Grover, O. Dmitriyeva, M. J. Estes, and G. Moddel, IEEE Trans. Nanotechnol. **9**(6), 716–722 (2010).

[24] M. N. Gadalla, M. Abdel-Rahman, and A. Shamim, Sci. Rep. **4**, 4270 (2014).

[25] N. Alimardani, S. W. King, B. L. French, C. Tan, B. P. Lampert, and J. F. Conley, J. Appl. Phys. **116**(2), 024508 (2014).

[26] S. Krishnan, E. Stefanakos, and S. Bhansali, Thin Solid Films **516**(8), 2244–2250 (2008).

[27] J. A. Bean, A. Weeks, and G. D. Boreman, IEEE J. Quantum Electron. **47**(1), 126–135 (2011).

[28] D. Vuillaume, P. Fontaine, J. Collet, D. Deresmes, M. Garet, and F. Rondelez, Microelectron. Eng. **22**(1), 101–104 (1993).

[29] C. Boulas, J. V. Davidovits, F. Rondelez, and D. Vuillaume, Phys. Rev. Lett. **76**(25), 4797–4800 (1996).

[30] D. Vuillaume, C. Boulas, J. Collet, J. V. Davidovits, and F. Rondelez, Appl. Phys. Lett. **69**(11), 1646–1648 (1996).

[31] F. Schreiber, Prog. Surf. Sci. **65**(5), 151–257 (2000).

[32] S. Casalini, C. A. Bortolotti, F. Leonardi, and F. Biscarini, Chem. Soc. Rev. **46**(1), 40–71 (2017).

[33] N. Padma, S. P. Koiry, V. Saxena, A. K. Chauhan, D. K. Aswal, S. K. Gupta, and J. V. Yakhmi, J. Nanosci. Nanotechnol. **9**(9), 5273–5277 (2009).

[34] S. K. Gupta, S. P. Koiry, A. K. Chauhan, N. Padma, D. K. Aswal, and J. V. Yakhmi, Appl. Surf. Sci. **256**(2), 407–413 (2009).

[35] S. A. Kulkarni and K. P. Vijayamohanan, Surf. Sci. **601**(14), 2983–2993 (2007).

[36] M. Lessel, O. Bäumchen, M. Klos, H. Hähl, R. Fetzer, M. Paulus, R. Seemann, and K. Jacobs, Surf. Interface Anal. **47**(5), 557–564 (2015).

[37] H. Fujiwara, *Spectroscopic Ellipsometry: Principles and Applications* (John Wiley & Sons Ltd, 2007).

[38] Z. Tang, H. Li, D. W. Hess, and V. Breedveld, Cellulose **23**(2), 1401–1413 (2016).

[39] A. A. Khan, G. Jayaswal, F. A. Gahaffar, and A. Shamim, Microelectron. Eng. **181**, 34–42 (2017).

[40] E. W. Cowell, S. W. Muir, D. A. Keszler, and J. F. Wager, J. Appl. Phys. **114**(21), 213703 (2013).